



Synergistic effects of phosphorous/sulfur co-doping and morphological regulation for enhanced photocatalytic performance of graphitic carbon nitride nanosheets

Xiaoxue Han¹, Aili Yuan¹, Chengkai Yao¹, Fengna Xi¹, Jiyang Liu¹, and Xiaoping Dong^{1,*}

¹Department of Chemistry, Zhejiang Sci-Tech University, 928 Second Avenue, Xiasha Higher Education Zone, Hangzhou 310018, China

Received: 6 July 2018

Accepted: 12 September 2018

Published online:
18 September 2018

© Springer Science+Business
Media, LLC, part of Springer
Nature 2018

ABSTRACT

Graphitic carbon nitride ($g\text{-C}_3\text{N}_4$) as a metal-free polymer semiconductor has received extensive attentions, but its application was drastically suppressed due to low photocatalytic activity. Herein, non-metal heteroatom co-doping is employed to extend the visible light absorption, and regulating morphology into nanosheets promotes the charge separation and transfer. Elements of P/S were successfully introduced into the carbon nitride framework by thermal condensation of their corresponding precursors with melamine. And, the presence of NH_4Cl would produce abundant gas to blow CN layers separately to form thin nanosheets. The obtained P/S co-doped carbon nitride nanosheet ($g\text{-PSCNNS}$) sample presents enhanced absorption in visible light region and efficiencies for separation and transport of photo-generated charges. The synergistic effect of elemental co-doping and nanosheet-like morphology endues $g\text{-PSCNNS}$ with superior photocatalytic performance for removal of organic pollutants in comparison with the pristine, P or S individual doped and P/S co-doped $g\text{-C}_3\text{N}_4$ samples. Moreover, this $g\text{-PSCNNS}$ sample has excellent photocatalytic stability and reusability. Experiments of radical quenching demonstrate superoxide radical is the main active species in the photocatalytic process.

Introduction

Recently, the growing awareness of the energy crisis and environmental pollution has encouraged extensive investigation of new clean energy to replace

traditional fossil fuels [1]. Semiconductor photocatalysis has emerged as one of the most fascinating research fields for eliminating organic pollutants and converting solar energy [2, 3]. A metal-free photocatalyst graphitic carbon nitride ($g\text{-C}_3\text{N}_4$) has attracted intensive interest for its promising applications in

Address correspondence to E-mail: xpdong@zstu.edu.cn

splitting water to produce H_2 [4–7], decomposition of organic pollutants [8], organic synthesis under visible light [9], photocatalytic CO_2 reduction [10] and photocatalytic NO removal [11–13]. The tunable condensation degree and distinctive heptazine ring structure endow $g-C_3N_4$ with good physicochemical stability as well as a fascinating electronic structure and a medium band gap (~ 2.7 eV) [14].

However, $g-C_3N_4$ has some shortcomings such as a low visible light utilization efficiency, small specific surface area and rapid recombination of photo-generated electron–hole pairs. To advance this photocatalyst, a number of researchers started to employ many strategies, for instance heteroatom doping including metal [15–18] and non-metal [19–41] elements, preparation of mesoporous $g-C_3N_4$ [42, 43], exfoliation of $g-C_3N_4$ into ultrathin nanosheets [44–46] and construction of heterojunctions with other semiconductors [47–49]. Among these strategies, non-metal dopants show great possibility to enhance the visible light photocatalysis of $g-C_3N_4$ via regulating the electronic structure and band gap [50, 51]. In recent years, various non-metal heteroatoms have been successfully introduced into the CN framework, such as O, F, S, P [19–23, 27–39]. Zhang et al. [23] prepared P-doped $g-C_3N_4$ using dicyandiamide and the ionic liquid [Bmim]PF₆ as the precursors. The electrical conductivity and the separation efficiency of photo-generated charges were obviously enhanced after P doping. Ge et al. [35] synthesized the S-doped $g-C_3N_4$ using thiourea as sulfur source. The sulfur-doped $g-C_3N_4$ photocatalysts show beneficial effects on visible light absorption, electron–hole pair generation and separation. Li et al. [38] synthesized O-doped $g-C_3N_4$ by a facile H_2O_2 hydrothermal approach. The O-doping process effectively enlarges surface area, extends visible light response and improves separation efficiency of the photo-induced charge carriers. Bao et al. [40] prepared the C-doped $g-C_3N_4$ that narrowed the band-gap, restrained the photo-induced charge carriers recombination and exhibited excellent photocatalytic performance. It should be noted, however, that single element doping always could not obtain the satisfactory photocatalytic properties and a few studies have utilized elemental co-doping strategies to further improve the photocatalytic performance of $g-C_3N_4$ [51–53].

Dimensionality plays the key role in determining the special properties of materials. As the graphite

analogue, CN is easy to form two-dimensional (2D) ultrathin structure, such as nanosheets [54, 55], nanoribbons [56] and nanoflakes [57]. These 2D materials have large surface area that provides more active sites and smaller sheet thickness that shortens the transfer route of photo-excited carriers. For example, Niu et al. [54] developed a simple method to prepare $g-C_3N_4$ nanosheets by direct thermal oxidation “etching” process of bulk $g-C_3N_4$ in air. The resultant nanosheets possess a large surface area and small sheet thickness and show much superior photocatalytic activities than the bulk $g-C_3N_4$.

In this study, we synthesized a P/S co-doped $g-C_3N_4$ nanosheet ($g-PSCNNS$) material by thermal polymerization of C, N, P and S precursors assisted with an NH_4Cl chemical blowing method. The structure and morphology were significantly changed by P/S co-doping in carbon nitride framework that results in the enhanced visible light absorption, good charge conductivity and high separation efficiency of photo-induced electron–hole pairs. We investigated the photocatalytic activity and durability of $g-PSCNNS$ for decomposing organic pollutants and finally proposed a possible photocatalytic mechanism.

Experimental section

Synthesis of photocatalysts

The $g-C_3N_4$ -based photocatalysts were synthesized by thermal condensation of various precursors with melamine, which are schematically illustrated in Fig. 1.

The pristine $g-C_3N_4$ ($g-CN$): A certain amount of melamine were poured into a crucible with a cover and heated in a muffle furnace at 520 °C for 4 h at a rate of 6 °C min⁻¹.

The S-doped $g-C_3N_4$ ($g-SCN$): Thiourea and melamine with a mass ratio of 1:1 were mixed in an agate mortar. Then, the mixture was treated similar to $g-CN$.

The P-doped $g-C_3N_4$ ($g-PCN$): 3 g melamine was added into 15 mL BmimPF₆ (50 mg) aqueous solution and then was heated at 100 °C under stirring to remove water. The white mixtures were treated following the procedure like $g-CN$.

The P/S co-doped $g-C_3N_4$ ($g-PSCN$): 3 g melamine and different amounts (25 mg, 50 mg, 75 mg,

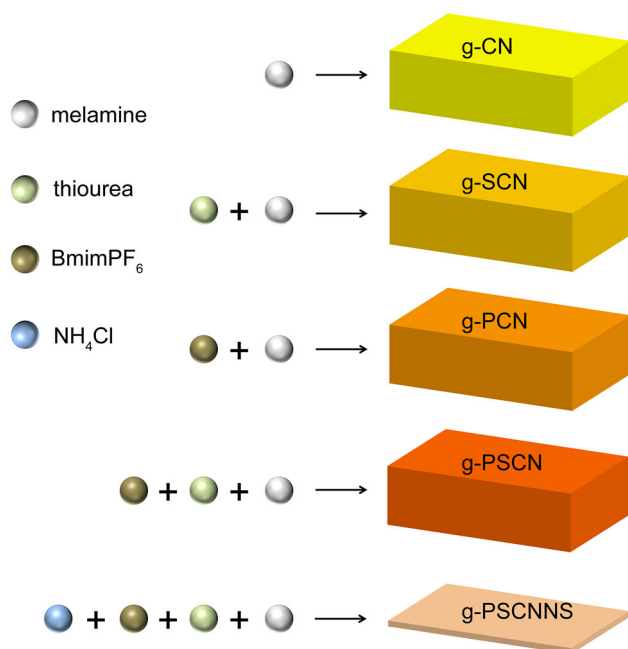


Figure 1 Schematic illustrations for preparation of **a** g-CN, **b** g-SCN, **c** g-PCN, **d** g-PSCN and **e** g-PSCNNS.

100 mg) of BmimPF₆ were added into 15 mL water under stirring. After removing water at 100 °C, the white resultants were mixed with 3 g thiourea in agate mortar. The mixture was then calcined at 520 °C for 4 h, and the prepared materials were referred to g-PSCN-25, g-PSCN-50, g-PSCN-75 and g-PSCN-100.

The P/S co-doped g-C₃N₄ nanosheets (g-PSCNNS): 3 g melamine and 50 mg BmimPF₆ were added into 15 mL water under stirring. After removing water at 100 °C, the powders were mixed with 3 g thiourea and 12 g NH₄Cl. Subsequently, treating with the similar process to g-PSCN, we obtained the sample of g-PSCNNS.

Characterizations

The morphology and composition of materials were analyzed by Quanta 250FEG Field emission scanning electron microscope (SEM) equipped with an energy-dispersive X-ray spectrometer (EDS). X-ray powder diffraction (XRD) patterns were measured using a DX-2700 diffractometer (Dandong Haoyuan Instrument Co. Ltd. China) using Cu K α radiation ($\lambda = 0.15418$ nm). Fourier transform infrared (FTIR) spectra were obtained on a Nicolet Avatar 370 spectrophotometer using the standard KBr disk method. UV–vis spectroscopy measurement was taken on a

Shimadzu 2450 UV–Vis spectrometer with an integrating sphere using BaSO₄ as the reference. X-ray photoelectron spectroscopy (XPS) was obtained on a VG K-ALPHA instrument with an Al K α monochromatic source. The electrochemical tests were performed on a CHI660E electrochemical workstation (Chenhua, Shanghai, China), and the detailed procedure is shown in Supporting Information. Photoluminescence (PL) spectra of the materials were measured using a fluorescence spectrophotometer with an excitation wavelength at 340 nm by Edinburgh FL/FS900 spectrophotometer.

Photocatalytic tests

The photocatalytic performance of materials was evaluated in a 150 mL reactor with a circulating water system by photocatalytic degradation of Rhodamine B (RhB) in aqueous solution under visible light irradiation which used a 300 W Xe lamp (HSX-F300, Beijing NBet) with a 420 nm cutoff filter as the light source. 0.1 g of catalyst and 100 mL of RhB aqueous solution (10 mg L⁻¹) were added in the reactor, and then the liquor was stirred in dark for 1 h to establish the adsorption–desorption equilibrium. During the photo-reaction process, 3.5 mL of the suspension was collected at the 20-min intervals and subsequently centrifuged to remove the catalyst particles. Then, centrifugal supernatant fluid was analyzed by measuring the maximum absorbance at 554 nm for RhB on a Shimadzu UV-2450 spectrophotometer.

Results and discussion

Physicochemical properties of photocatalysts

SEM images were used to observe the morphological change of photocatalysts by elemental doping and chemical blowing (Fig. 2). As shown in Fig. 2a, the pristine g-CN sample exhibits an irregular particulate shape with a size of several micrometers. The introduction of P/S heteroatoms into g-C₃N₄ skeleton does not apparently alter its aspect, which is confirmed by the SEM photograph of g-PSCN (Fig. 2b). With the presence of NH₄Cl in the synthetic process, the chemical blowing effect would suppress the ordered stacking of CN layers and result in a loose

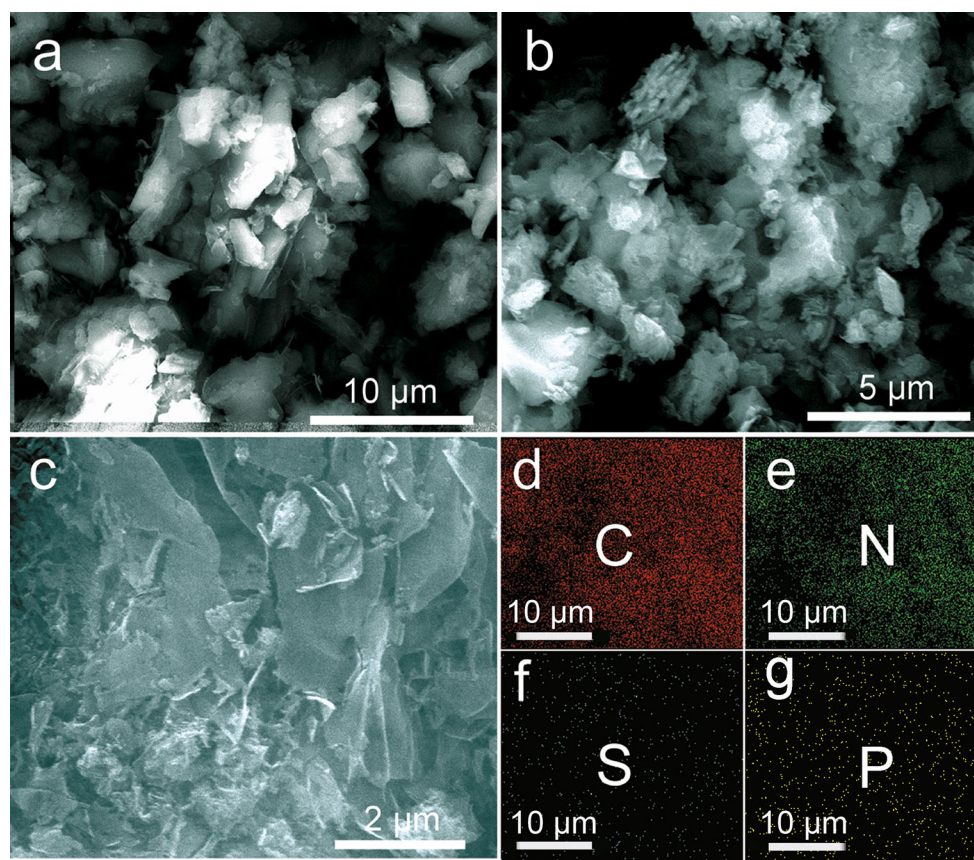


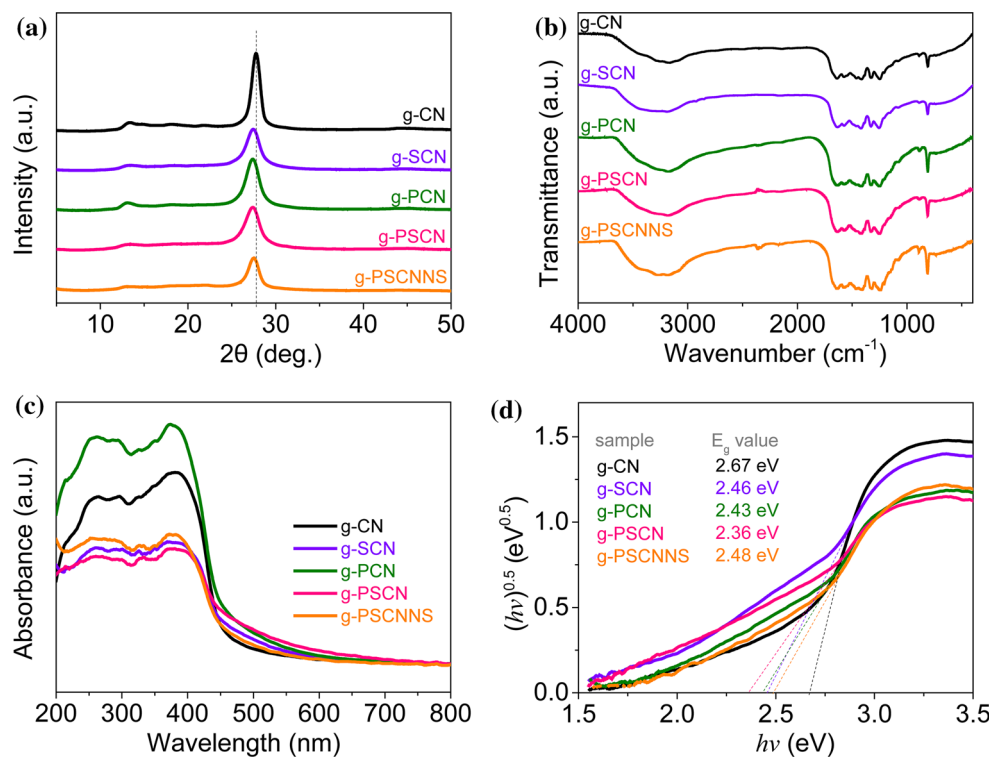
Figure 2 SEM images of **a** g-CN, **b** g-PSCN and **c** g-PSCNNS; EDS elemental mapping images of **d** C, **e** N, **f** S and **g** P in g-PSCNNS.

aggregation of few-layer structures. This will result in an enhanced specific surface area for g-PSCNNS compared to g-CN and g-PSCN samples (Fig. S1 and Table S1). We can find from Fig. 2c that the g-PSCNNS sample displays a typical 2D nanosheet-like morphology, and the curled edges in these sheets indicate their flexibility and ultrathin thickness. The elemental mappings of g-PSCNNS by EDS are depicted in Fig. 2d–g. Four elements, C, N, S and P, were checked, and all of them are uniformly distributed in the g-PSCNNS sample. This result suggests that P/S elements have been successfully doped into the CN framework.

The crystal structure of samples was studied by XRD technique, as shown in Fig. 3a. All the patterns reveal two distinct peaks, respectively, corresponding to (100) diffraction at 13.0° and (002) diffraction at 27.5° [22, 61]. The former is related to the in-planar ordered alignment of tri-s-triazine units, and the latter results from the oriented stacking of 2D CN layers [22, 61]. In comparison with the pristine g-CN, the intensity of these diffractions evidently decreases in

the heteroatom-doped samples, g-SCN, g-PCN and g-PSCN. This result may be attributed to the lattice distortion after doping heteroatom into CN framework. With the treatment of NH_4Cl chemical blowing, the (002) peak of g-PSCNNS further weakens and widens, which is assigned to the diminished thickness. Furthermore, it is evidently found that the (002) diffraction in these doped samples has a slight shift to the low degree zone compared to g-CN. This enlargement of interlayer space after doping heteroatoms can be attributed to the much larger atom radius of S and P than those of C and N. FTIR spectra were measured to characterize functional groups of samples (Fig. 3b). A series of typical absorption peaks in the region of $1200\text{--}1700\text{ cm}^{-1}$ are attributed to the typical stretching modes of CN heterocycles [49]. The sharp peak is located at 809 cm^{-1} owing to a breathing mode of s-triazine ring system. The broad absorption band over $2900\text{ to }3500\text{ cm}^{-1}$ is arising from the N–H and N–H₂ stretching vibrations [46, 52]. No apparent difference is observed in these

Figure 3 **a** XRD patterns, **b** FTIR spectra, **c** UV–vis absorption spectra and **d** Tauc plots of photocatalysts.



spectra, indicating that introduction of dopants does not affect the CN heterocycle structure.

Optical properties of these different $g\text{-C}_3\text{N}_4$ samples were investigated by UV–vis DRS (Fig. 3c). The yellow pristine $g\text{-CN}$ presents an intensive absorption beginning from 454 nm, and the band gap (E_g) estimated from Tauc plot (Fig. 3d) is 2.67 eV that is similar to the reported value [14, 35, 45, 49]. Doping with P/S, absorption in visible region is significantly strengthens, and the color darkens for $g\text{-SCN}$, $g\text{-PCN}$ and $g\text{-PSCN}$, implying that heteroatoms-doped samples have much more sufficient utilization of solar light than the pristine $g\text{-CN}$. The redshift of absorption edge causes the reduction in band gaps, which are 2.46, 2.43 and 2.36 eV for $g\text{-SCN}$, $g\text{-PCN}$ and $g\text{-PSCN}$, respectively. As for $g\text{-PSCNNS}$, its absorption edge has a slight blueshift compared to $g\text{-PSCN}$ because of its thin thickness. The evaluated E_g value of $g\text{-PSCNNS}$ is 2.48 eV.

XPS technology was employed to investigate the elemental composition and chemical state of $g\text{-PSCNNS}$. The survey spectrum (Fig. 4a) presents the presence of C, N, O, S and P, and the atomic ratios of S and P are 0.32% and 0.22%, respectively. Figure 4b illustrates the C 1s spectrum of $g\text{-PSCNNS}$ that is fitted into three typical peaks. Among them, the signal at a binding energy of 284.6 eV is ascribed

to adventitious carbon contamination (C–C and C=C), the peak located at 286.0 eV corresponds to the C–OH environment, and the sp^2 C atoms in N-containing aromatic skeleton rings (N–C=N) are responsible for the band at 288.2 eV [51, 52, 59]. The N 1s spectrum of $g\text{-PSCNNS}$ can be divided into three peaks, as displayed in Fig. 4c. The main peak at 398.8 eV is related to the sp^2 N atoms in conjugated CN ring, and two shoulder peaks at 399.6 and 400.8 eV are, respectively, assigned to N–(C)₃ and N–H groups [51, 52]. The symmetric O 1s spectrum (Fig. 4d) centered at 532.6 eV suggests the single source of O element that is contributed from adsorbed water [51]. The S 2p peak (Fig. 4e) was deconvoluted into two bands at 165.4 and 167.5 eV. The peak at 165.4 eV is attributed to the N–S bond that is formed by substituting sulfur with lattice carbon [58]. And, the band at 167.5 eV can be ascribed to the oxidized S (SO_x) that is modified on CN layers [59]. Figure 4f exhibits the P 2p spectrum of $g\text{-PSCNNS}$ that is located at 133.9 eV, which corresponds to P–N coordination, implying that P most probably substitutes for C in triazine rings [60, 61]. All the above results demonstrate S and P have been successfully doped into the carbon nitride framework.

Electrochemical impedance spectra (EIS) and photocurrent measurements are useful tools for

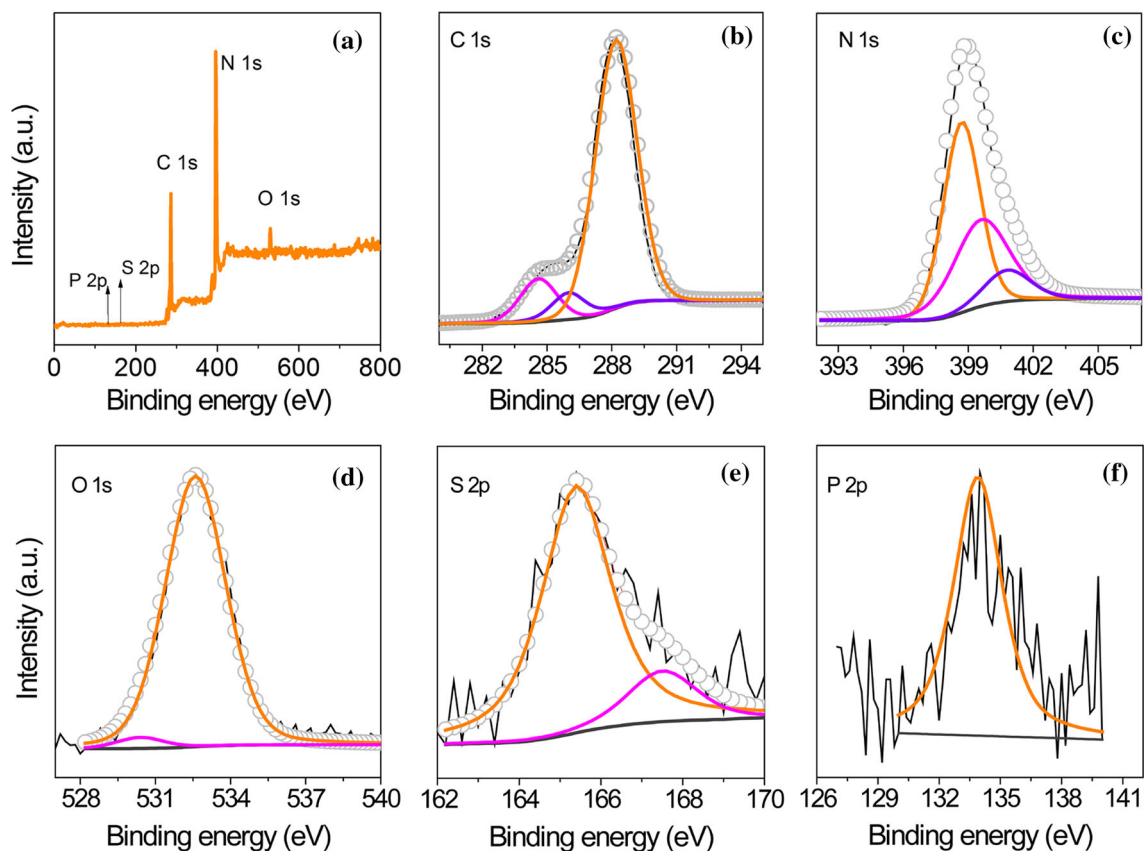


Figure 4 XPS spectra of g-PSCNNS: **a** survey; **b** C 1s, **c** N 1s, **d** O 1s, **e** S 2p and **f** P 2p.

characterizing the separation and migration ability of photo-excited charges. Figure 5a shows the EIS data of g-CN, g-SCN, g-PCN, g-PSCN and g-PSCNNS electrodes. Obvious semi-circles are found in these curves, and their diameters reflect the resistance of charge transfer (R_{ct}) at the solid/liquid interface [62]. These heteroatoms-doped samples have much smaller semi-circles than the pristine g-CN, revealing their much more efficient migration and transfer ability of

photo-generated carriers. The nanosheet morphology provides a short route for photo-induced electrons and holes to diffuse to surface, which results in the further decrease in R_{ct} for g-PSCNNS sample. Transient photocurrent response also gives a similar result, as presented in Fig. 5b. The highest photocurrent density is achieved by the g-PSCNNS sample, suggesting its most efficient separation of photo-excited charges among these samples. In

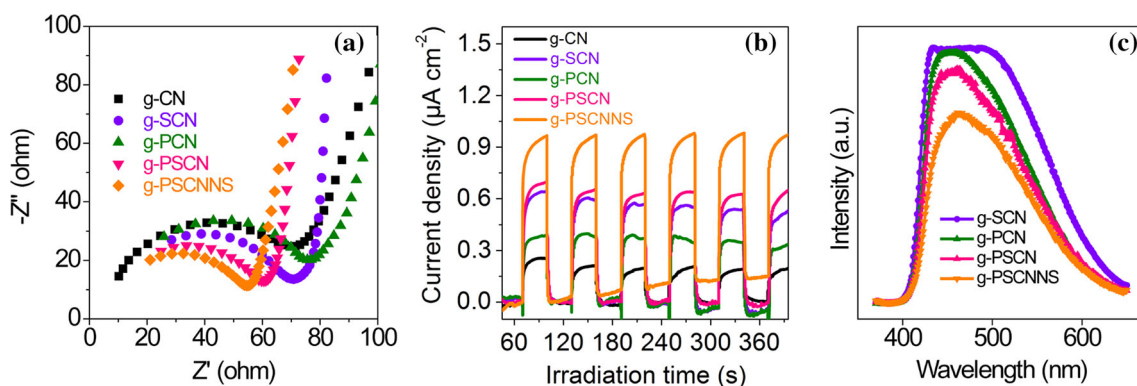


Figure 5 **a** Nyquist plots of EIS, **b** photocurrent responses and **c** PL spectra of photocatalysts.

addition, several repeated on–off cycles exhibit similar photocurrent response. It implies the high photostability of samples. The recombination of photo-produced electron–hole pairs in photocatalysts would produce fluorescent emission. Figure 5c illustrates PL spectra of heteroatom-doped samples, where g-PSCNNS shows the most weak PL intensity, demonstrating the highest charge separation efficiency in g-PSCNNS sample.

Synergistic effects for enhancing photocatalytic performance of g-PSCNNS

The photocatalytic activity of samples was studied by degradation of RhB under visible light irradiation. We firstly optimized the doping of P/S by tuning the dosage of P precursor (25, 50, 75 and 100 mg) in synthetic procedure without adding NH_4Cl . It is obvious that the introduction of appropriate P is favorable for promoting photocatalytic performance; however, excessive P will suppress the activity of P/S co-doped samples (Fig. 6a). Similar photocatalytic behavior is found for the samples using 50 mg and 75 mg P precursor. Considering the relative high cost of BmimPF_6 , we chose 50 mg as the optimal dosage. Figure 6b compares the photocatalytic activity of various carbon nitride samples. Due to the insufficient utilization of visible light and high recombination rate of photo-generated electron–hole pairs, the pristine g-CN shows a poor activity, and only 50% RhB was removed after 120 min irradiation. Activity enhancement is achieved by introducing P or S elements in graphitic carbon nitride, and the g-PCN and g-SCN, respectively, give 58% and 82% degradation efficiency after 120 min. The co-doped g-PSCN sample even can completely photo-degrade dye molecules. By chemical blowing of g-PSCN into nanosheets, the g-PSCNNS sample displays a significant adsorption capability. It should be induced by the enhanced surface area of nanosheet morphology. And, the g-PSCNNS sample presents a more prominent activity than g-PSCN that photo-decomposes all of RhB after 40 min visible light illumination. The color change of reaction system (Fig. S2) and the DRS of photocatalysts before and after photocatalysis reaction (Fig. S3) suggest that the adsorbed dyes on g-PSCNNS were also completely removed. To further understand the reaction rate of degradation, the photocatalytic kinetic study was investigated by the pseudo-first-order model with the following

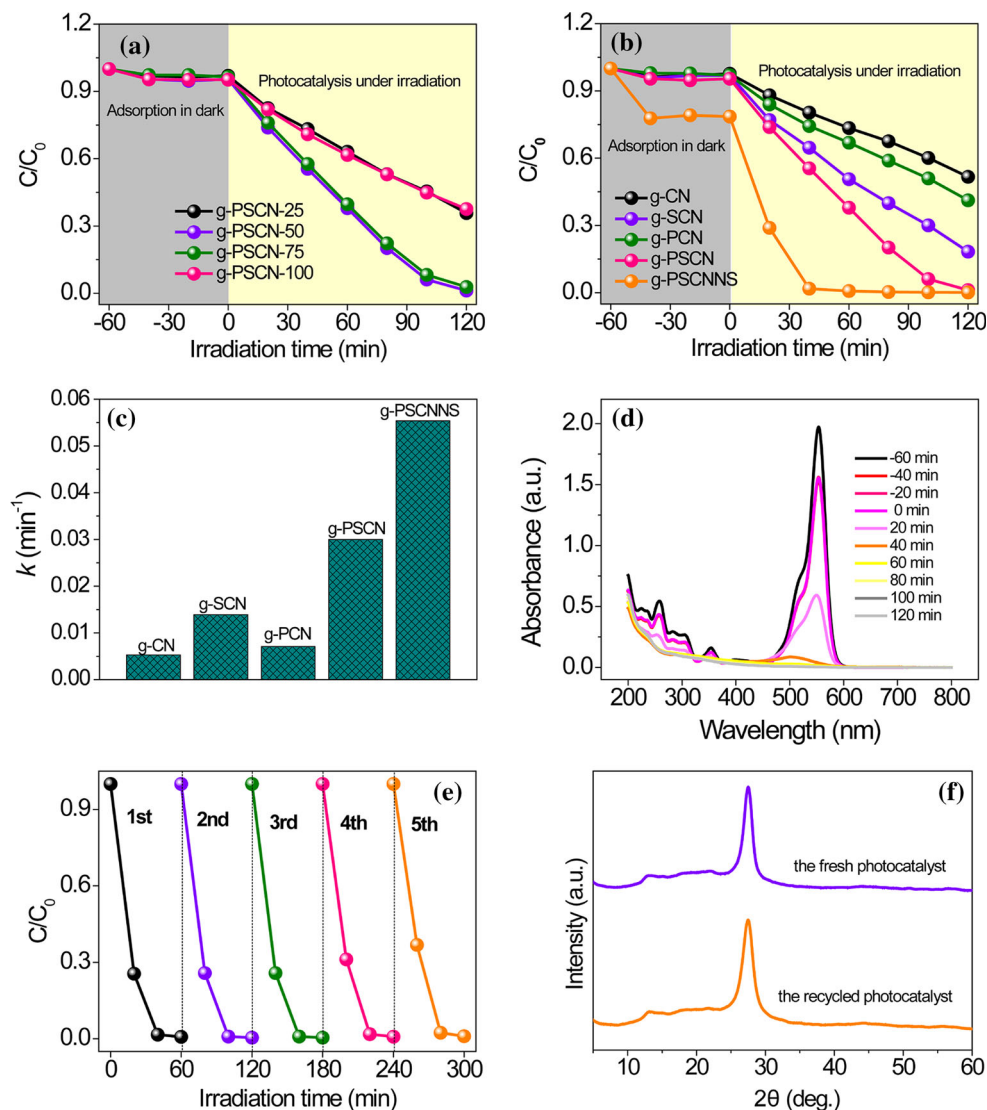
equation: $\ln(C_0/C) = k \times t$, where C_0 is the initial RhB concentration after establishing adsorption–desorption equilibrium, C is the remaining concentration at irradiation time of t , and k is the apparent first-order rate constant [63]. As shown in Fig. 6c, the g-PSCNNS exhibits the largest rate constant k of 0.0554 min^{-1} that is ~ 10.5 , 4.0, 7.8 and 1.9 times higher than those of g-CN, g-SCN, g-PCN and g-PSCN, respectively.

Figure 6d depicts the absorption spectral change of RhB solution with the presence of g-PSCNNS under visible light irradiation. Besides rapid decay of the main absorption at 554 nm, no apparent blueshift is observed, demonstrating the simultaneous removal of all the ethyl groups on RhB molecule [64, 65]. Meanwhile, absorptions in UV region also decrease with the increase in illumination time. It can be assigned to the destruction of aromatic ring in RhB [65]. The supernatant after photocatalytic reaction was examined by high-performance liquid chromatography (HPLC). As Table S2 reveals, RhB was completely decomposed and the main intermediates were determined as oxalic acid (OA) and fumaric acid (FA).

The stability and reusability of g-PSCNNS photocatalyst for degradation of RhB were examined by adding concentrated dye solution into the photocatalytic system after the previous cycle. Figure 6e displays the successive five cycle experiments of the g-PSCNNS sample. No evident decline of activity is observed, revealing the superior reusability of g-PSCNNS. Figure 6f shows the comparison of XRD patterns of g-PSCNNS before and after photocatalytic reaction. The (100) and (002) diffractions are still maintained after reaction, which proves the high stability of g-PSCNNS photocatalyst. We also compared the photocatalytic performance of g-PSCNNS with the pristine g-CN for removal of various organic dyes, including methyl blue (MB), Reactive violet and Congo red under visible light irradiation (Fig. S4), where the g-PSCNNS presents better photocatalytic performance than that of the pristine g-CN.

As described by optical behaviors of carbon nitride materials in Fig. 3c and d, heteroatom dopants will significantly change their band structure. To investigate the detailed band alignment, Mott–Schottky (MS) measurements were taken, and the resultant data are illustrated in Fig. 7a–e. All the heteroatom-doped samples have a positive slope of MS curves like the pristine g-CN, indicating they are all n-type

Figure 6 Visible light photocatalytic performance of photocatalysts for degradation of RhB: **a** the influence of P content on activity; **b** photocatalytic RhB removal ratio by various photocatalysts and **c** their corresponding apparent rate constants; **d** UV–vis absorption spectral change of RhB solution by the photocatalysis of g-PSCNNS; **e** the cycle behaviors of g-PSCNNS; **f** XRD patterns of g-PSCNNS before and after photocatalytic reaction.



semiconductors and these dopants do not influence the conduction behavior [66]. Their flat potentials estimated from the intercept at X-axis are, respectively, -1.48 , -1.28 , -1.04 , -0.97 and -1.05 eV versus Ag/AgCl for g-CN, g-SCN, g-PCN, g-PSCN and g-PSCNNS. Based on their E_g values, we subsequently plotted the band alignment in Fig. 7f. When reducing band gap by doping with P or S heteroatoms, it simultaneously effectively shifts the conduction band (CB) potential to positive potential. And, the much more obvious effect is realized by the co-doped sample of g-PSCN. Furthermore, compared to g-PSCN, the CB and valence band (VB) of g-PSCNNS, respectively, shift to more negative and positive direction.

In photocatalytic oxidation process, photo-generated holes, superoxide radical ($\cdot\text{O}_2^-$) and hydroxyl radical ($\cdot\text{OH}$) are three main active species. To reveal the main species in this system, we investigated the influence of photocatalytic performance by introducing various scavengers. As shown in Fig. 8a, when tert-butyl alcohol (TBA, 2 mM, a scavenger of hydroxyl radicals) was added, the degradation efficiency of RhB was changed slightly [45, 46, 63]. This result demonstrates that $\cdot\text{OH}$ radicals were not involved in the photocatalytic process. However, the addition of scavenger benzoquinone (BQ, 0.5 mM) for $\cdot\text{O}_2^-$ radicals, the degradation behavior of RhB was seriously prohibited, which suggests that $\cdot\text{O}_2^-$ radicals are the main active species in the photocatalytic process [45, 46, 63]. Disodium

Figure 7 a–e Mott–Schottky curves and f schematic diagram for band alignment of photocatalysts.

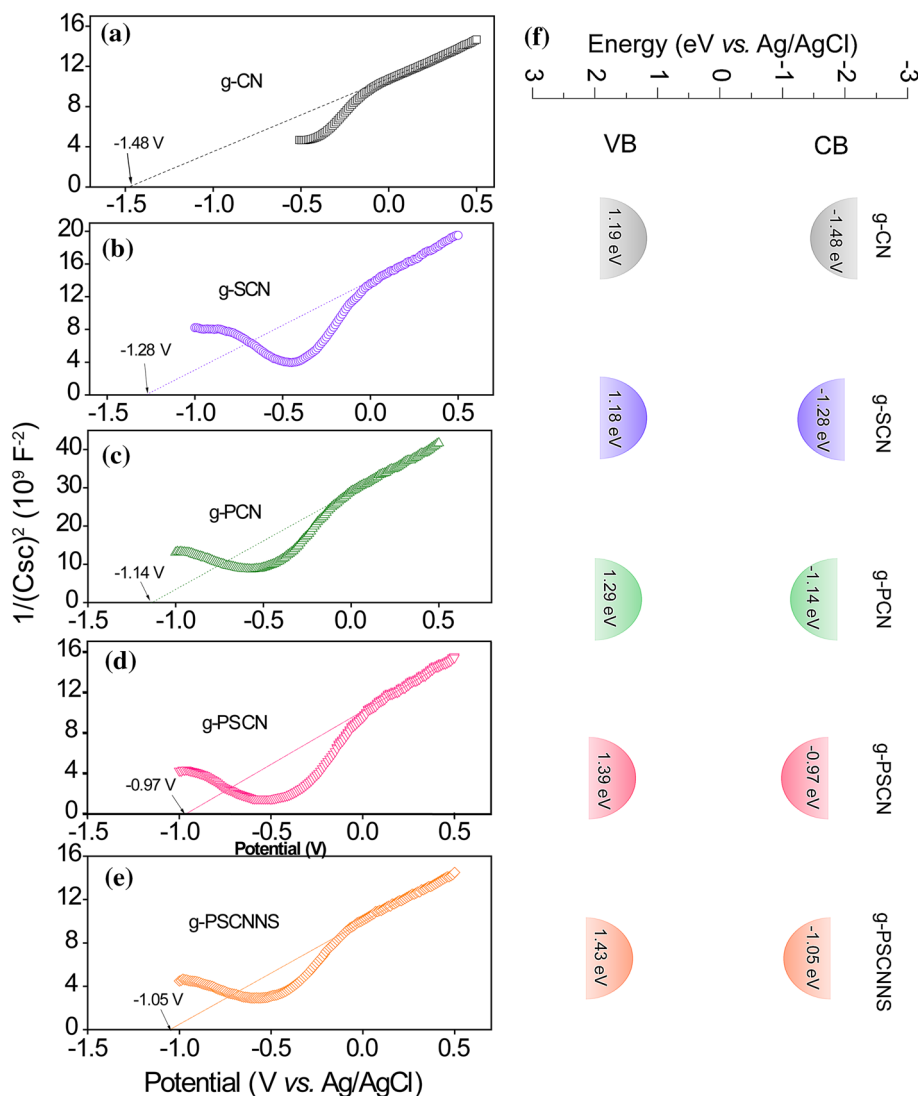
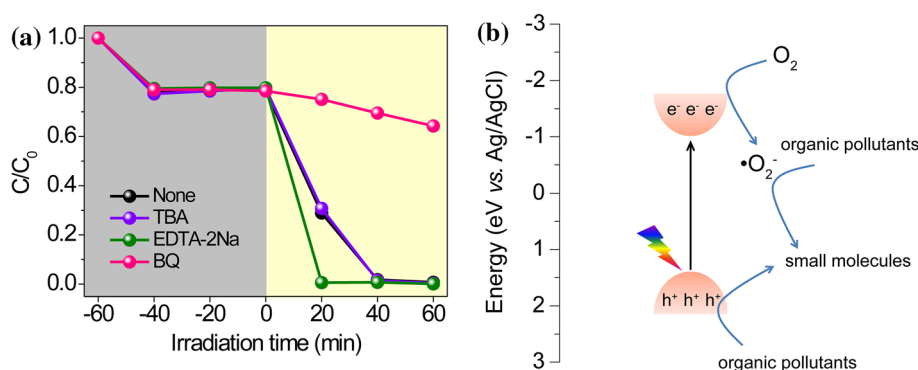


Figure 8 a The photocatalytic activity of g-PSCNNS for degrading RhB with the presence of various scavengers, and b the possible photocatalytic mechanism of g-PSCNNS under visible light irradiation.



ethylenediaminetetraacetate (EDTA-2Na, 2 mM) was used to trap photo-excited holes on VB [45, 46, 63]. The removal efficiency of RhB was not diminished, but increased. That should be contributed by the

enhanced separation rate of photo-generated carriers by quenching holes.

According to the above results, a possible mechanism for photo-degradation of organic dyes by g-PSCNNS is therefore proposed that is schematically

illustrated in Fig. 8b. Under visible light illumination, the electrons (e^-) on VB are excited and transferred to CB, meanwhile leaving the positively charged holes (h^+) on VB. The high recombination of e^-h^+ pairs results in the inefficient activity of g-CN, however, which is markedly suppressed in g-PSCNNS because its extremely thin morphology provides a short distance for carriers to diffuse to surface. Subsequently, the photo-induced electrons on CB are trapped by the defects on surface and then react with the dissolved oxygen to produce $\cdot O_2^-$. On the other hand, the VB potential is much more negative than the $H_2O/\cdot OH$ redox potential (1.43 V vs. NHE) [46]. Thus, the photo-generated holes cannot oxidize H_2O to $\cdot OH$. However, they can directly oxidize RhB because of the relatively small oxidizing potential of RhB (0.97 V vs. NHE) [67].

Conclusion

In summary, a simultaneous approach of binary heteroatom co-doping and 2D morphological controlling was employed to promote the photocatalytic performance of graphitic carbon nitride. Co-doping heteroatoms of P/S into the CN skeleton diminished the optical gap that means harvesting more sunlight, and meanwhile prohibited the charge recombination and improved its conductivity. What is more, blowing CN layers separately into nanosheet-like morphology enhanced the surface concentration of active sites and further promoted the separation of photo-excited carriers by shortening their diffusion distance to surface. These synergistic effects brought g-PSCNNS much more excellent photocatalytic behavior than these reference samples for comparison. Also, this photocatalyst has a well stability and can be repeatedly used for successive cycles. We believe this strategy is a common route to synthesize multi-heteroatoms-doped g- C_3N_4 photocatalysts with 2D ultrathin structure. Furthermore, its flexible 2D morphology is helpful for fabricating tightly coupled heterostructure photocatalysts by encapsulating guests into nanosheets.

Acknowledgements

This work was financially supported from the financial support from the Zhejiang Provincial

Natural Science Foundation of China (No. LY17B010004, LY17B050007) and the 521 talent Project of ZSTU.

Electronic supplementary material: The online version of this article (<https://doi.org/10.1007/s10853-018-2925-9>) contains supplementary material, which is available to authorized users.

References

- [1] Chen C, Ma W, Zhao J (2010) Semiconductor-mediated photodegradation of pollutants under visible-light irradiation. *Chem Soc Rev* 39:4206–4219
- [2] Liu G, Wang L, Yang H, Cheng H, Lu G (2010) Titania-based photocatalysts-crystal growth, doping and heterostructuring. *J Mater Chem* 20:831–843
- [3] Zhang D, Li G, Yu J (2010) Inorganic materials for photocatalytic water disinfection. *J Mater Chem* 20:4529–4536
- [4] Zhang J, Zhang G, Chen X, Lin S, Mohlmann L, Lipner G, Antonietti M, Blechert S, Wang X (2012) Co-monomer control of carbon nitride semiconductors to optimize hydrogen evolution with visible light. *Angew Chem Int Ed* 51:3183–3187
- [5] Cao S, Li H, Tong T, Chen H, Yu A, Yu J, Chen H (2018) Single-atom engineering of directional charge transfer channels and active sites for photocatalytic hydrogen evolution. *Adv Funct Mater* 28:1802169–1802177
- [6] Cao S, Huang Q, Zhu B, Yu J (2017) Trace-level phosphorus and sodium co-doping of g- C_3N_4 for enhanced photocatalytic H_2 production. *J Power Sources* 351:151–159
- [7] Jiang J, Cao S, Hu C, Chen C (2017) A comparison study of alkali metal-doped g- C_3N_4 for visible-light photocatalytic hydrogen evolution. *Chin J Catal* 38:1981–1989
- [8] Bu Y, Chen Z, Li W (2014) Using electrochemical methods to study the promotion mechanism of the photoelectric conversion performance of Ag-modified mesoporous g- C_3N_4 heterojunction material. *Appl Catal B Environ* 144:622–630
- [9] Xu J, Wu H, Wang X, Xue B, Li Y, Cao Y (2013) A new and environmentally benign precursor for the synthesis of mesoporous g- C_3N_4 with tunable surface area. *Phys Chem Chem Phys* 15:4510–4517
- [10] Cao S, Li Y, Zhu B, Jaroniec M, Yu J (2017) Facet effect of Pd cocatalyst on photocatalytic CO_2 reduction over g- C_3N_4 . *J Catal* 349:208–217
- [11] Cui W, Li J, Sun Y, Wang H, Jiang G, Lee S, Dong F (2018) Enhancing ROS generation and suppressing toxic intermediate production in photocatalytic NO oxidation on O/Ba co-

- functionalized amorphous carbon nitride. *Appl Catal B Environ* 237:938–946
- [12] Xiong T, Wang H, Zhou Y, Sun Y, Cen W, Huang H, Zhang Y, Dong F (2018) KCl-mediated dual electronic channels in layered g-C₃N₄ for enhanced visible light photocatalytic NO removal. *Nanoscale* 10:8066–8074
- [13] Dong X, Li J, Xing Q, Zhou Y, Huang H, Dong F (2018) The activation of reactants and intermediates promotes the selective photocatalytic NO conversion on electron-localized Sr-intercalated g-C₃N₄. *Appl Catal B Environ* 232:69–76
- [14] Wang X, Maeda K, Thomas A, Takanabe K, Xin G, Carlsson J, Domen K, Antonietti M (2009) A metal-free polymeric photocatalyst for hydrogen production from water under visible light. *Nat Mater* 8:76–80
- [15] Zhang M, Bai X, Liu D, Wang J, Zhu Y (2015) Enhanced catalytic activity of potassium-doped graphitic carbon nitride induced by lower valence position. *Appl Catal B Environ* 164:77–81
- [16] Wang Y, Zhao S, Zhang Y, Fang J, Zhou Y, Yuan S, Zhang C, Chen W (2018) One-pot synthesis of K-doped g-C₃N₄ nanosheets with enhanced photocatalytic hydrogen production under visible-light irradiation. *Appl Surf Sci* 440:258–265
- [17] Tonda S, Kumar S, Kandula S, Shanker V (2014) Fe-doped and-mediated graphitic carbon nitride nanosheets for enhanced photocatalytic performance under natural sunlight. *J Mater Chem A* 2(19):6772–6780
- [18] Bu Y, Chen Z, Li W (2014) Using electrochemical methods to study the promotion mechanism of the photoelectric conversion performance of Ag-modified mesoporous g-C₃N₄ heterojunction material. *Appl Catal B Environ* 144:622–630
- [19] Zhang Y, Mori T, Ye J, Antonietti M (2010) Phosphorus doped carbon nitride solid: enhanced electrical conductivity and photocurrent generation. *J Am Chem Soc* 132:6294–6295
- [20] Ma T, Ran J, Dai S, Jaroniec M, Qiao S (2015) Phosphorus-doped graphitic carbon nitrides grown in situ on carbon-fiber paper: flexible and reversible oxygen electrodes. *Angew Chem Int Ed* 54:4646–4650
- [21] Hu S, Ma L, You J, Li F, Fan Z, Wang F, Liu D, Gui J (2014) A simple and efficient method to prepare a phosphorus modified g-C₃N₄ visible light photocatalyst. *RSC Adv* 4:21657–21663
- [22] Zhou Y, Zhang L, Liu J, Fan X, Wang B, Wang M, Ren W, Wang J, Li M, Shi J (2015) Brand new P-doped g-C₃N₄ enhanced photocatalytic activity for H₂ evolution and rhodamine B degradation under visible light. *J Mater Chem A* 3:3862–3867
- [23] Zhang L, Chen X, Guan J, Jiang Y, Hou T, Mu X (2013) Facile synthesis of phosphorus doped graphitic carbon nitride polymers with enhanced visible-light photocatalytic activity. *Mater Res Bull* 48:3485–3491
- [24] Yan S, Li Z, Zou Z (2010) Photodegradation of rhodamine B and methyl orange over boron-doped g-C₃N₄ under visible light irradiation. *Langmuir* 26:3894–3901
- [25] Gao D, Liu Y, Liu P, Si M, Xue D (2016) Atomically thin B doped g-C₃N₄ nanosheets: high-temperature ferromagnetism and calculated half-metallicity. *Sci. Rep* 6:35768–35774
- [26] Sagara N, Kamimura S, Tsubota T, Ohno T (2016) Photoelectrochemical CO₂ reduction by a p-type boron doped g-C₃N₄ electrode under visible light. *Appl Catal B Environ* 192:193–198
- [27] Hong J, Xia X, Wang Y, Xu R (2012) Mesoporous carbon nitride with in situ sulfur doping for enhanced photocatalytic hydrogen evolution from water under visible light. *J Mater Chem* 22:15006–15012
- [28] Ye L, Chen S (2016) Fabrication and high visible-light-driven photocurrent response of g-C₃N₄ films: the role of thiourea. *Appl Surf Sci* 389:1076–1083
- [29] Liu G, Niu P, Sun C, Smith S, Chen Z, Lu G, Cheng H (2010) Unique electronic structure induced high photoreactivity of sulfur-doped graphitic C₃N₄. *J Am Chem Soc* 132:11642–11648
- [30] Cao L, Wang R, Wang D (2015) Synthesis and characterization of sulfur self-doped g-C₃N₄ with efficient visible-light photocatalytic activity. *Mater Lett* 149:50–53
- [31] Chen J, Hong Z, Chen Y, Lin B, Gao B (2015) One-step synthesis of sulfur-doped and nitrogen-deficient g-C₃N₄ photocatalyst for enhanced hydrogen evolution under visible light. *Mater Lett* 145:129–132
- [32] Seredych M, Bandosz T (2016) Nitrogen enrichment of S doped nanoporous carbon by g-C₃N₄: insight into photosensitivity enhancement. *Carbon* 107:895–906
- [33] Hong J, Xia X, Wang Y, Xu R (2012) Mesoporous carbon nitride with in situ sulfur doping for enhanced photocatalytic hydrogen evolution from water under visible light. *J Mater Chem* 22:15006–15012
- [34] Stolbov S, Zuluaga S (2013) Sulfur doping effects on the electronic and geometric structures of graphitic carbon nitride photocatalyst: insight from first principles. *J Phys Condens Matter* 25. <https://doi.org/10.1088/0953-8984/25/8/085507>
- [35] Ge L, Han C, Xiao X, Guo L, Li Y (2013) Enhanced visible light photocatalytic hydrogen evolution of sulfur-doped polymeric g-C₃N₄ photocatalysts. *Mater Res Bull* 48:3919–3925
- [36] Li L, Fang W, Zhang P, Bi J, He Y, Wang J, Su W (2016) Sulfur-doped covalent triazine-based frameworks for enhanced photocatalytic hydrogen evolution from water under visible light. *J Mater Chem A* 4:12402–12406

- [37] Huang Z, Song J, Pan L, Wang Z, Zhang X, Zou J, Mi W, Zhang X, Wang L (2015) Carbon nitride with simultaneous porous network and O-doping for efficient solar-energy-driven hydrogen evolution. *Nano Energy* 12:646–656
- [38] Li J, Shen B, Hong Z, Lin B, Gao B, Chen Y (2012) A facile approach to synthesize novel oxygen-doped g-C₃N₄ with superior visible-light photoreactivity. *Chem Commun* 48:12017–12019
- [39] Dong G, Ai Z, Zhang L (2014) Efficient anoxic pollutant removal with oxygen functionalized graphitic carbon nitride under visible light. *RSC Adv* 4:5553–5560
- [40] Bao N, Hu X, Zhang Q, Miao X, Jie X, Zhou S (2017) Synthesis of porous carbon-doped g-C₃N₄ nanosheets with enhanced visible-light photocatalytic activity. *Appl Surf Sci* 403:682–690
- [41] Fang J, Fan H, Li M, Long C (2015) Nitrogen self-doped graphitic carbon nitride as efficient visible light photocatalyst for hydrogen evolution. *J Mater Chem A* 3:13819–13826
- [42] Shi L, Liang L, Wang F, Liu M, Zhong S, Sun J (2015) Tetraethylorthosilicate induced preparation of mesoporous graphitic carbon nitride with improved visible light photocatalytic activity. *Catal Commun* 59:131–135
- [43] Hao R, Wang G, Tang H, Sun L, Xu C, Han D (2016) Template-free preparation of macro/mesoporous g-C₃N₄/TiO₂ heterojunction photocatalysts with enhanced visible light photocatalytic activity. *Appl Catal B Environ* 187:47–58
- [44] Lin Q, Li L, Liang S, Liu M, Bi J, Wu L (2015) Efficient synthesis of monolayer carbon nitride 2D nanosheet with tunable concentration and enhanced visible-light photocatalytic activities. *Appl Catal B Environ* 163:135–142
- [45] Yan J, Han X, Zheng X, Qian J, Liu J, Dong X, Xi F (2017) One-step template/chemical blowing route to synthesize flake-like porous carbon nitride photocatalyst. *Mater Res Bull* 94:423–427
- [46] Yan J, Han X, Qian J, Liu J, Dong X, Xi F (2017) Preparation of 2D graphitic carbon nitride nanosheets by a green exfoliation approach and the enhanced photocatalytic performance. *J Mater Sci* 52:13091–13102. <https://doi.org/10.1007/s10853-017-1419-5>
- [47] Qiu P, Yao J, Chen H, Jiang F, Xie X (2016) Enhanced visible-light photocatalytic decomposition of 2,4-dichlorophenoxyacetic acid over ZnIn₂S₄/g-C₃N₄ photocatalyst. *J Hazard Mater* 317:158–168
- [48] Zhang L, Jing D, She X, Liu H, Yang D, Lu Y, Li J, Zheng Z, Guo L (2014) Heterojunctions in g-C₃N₄/TiO₂(-B) nanofibres with exposed (001) plane and enhanced visible-light photoactivity. *J Mater Chem A* 2:2071–2078
- [49] Fu J, Chang B, Tian Y, Xi F, Dong X (2013) Novel C₃N₄-CdS composite photocatalysts with organic-inorganic heterojunctions: in situ synthesis, exceptional activity, high stability and photocatalytic mechanism. *J Mater Chem A* 1:3083–3090
- [50] Dong G, Zhao K, Zhang L (2012) Carbon self-doping induced high electronic conductivity and photoreactivity of g-C₃N₄. *Chem Commun* 48:6178–6180
- [51] You R, Dou H, Chen L, Zheng S, Zhang Y (2017) Graphitic carbon nitride with S and O codoping for enhanced visible light photocatalytic performance. *RSC Adv* 7:15842–15850
- [52] Wang H, Wang B, Bian Y, Dai L (2017) Enhancing photocatalytic activity of graphitic carbon nitride by codoping with P and C for efficient hydrogen generation. *ACS Appl Mater Interfaces* 9:21730–21737
- [53] Ma H, Li Y, Li S, Liu N (2015) Novel PO codoped g-C₃N₄ with large specific surface area: hydrothermal synthesis assisted by dissolution-precipitation process and their visible light activity under anoxic conditions. *Appl Surf Sci* 357:131–138
- [54] Niu P, Zhang L, Liu G, Cheng H (2012) Graphene-like carbon nitride nanosheets for improved photocatalytic activities. *Adv Funct Mater* 22:4763–4770
- [55] Zhang X, Xie X, Wang H, Zhang J, Pan B, Xie Y (2013) Enhanced photoresponsive ultrathin graphitic-phase C₃N₄ nanosheets for bioimaging. *J Am Chem Soc* 135:18–21
- [56] Zhao Y, Zhao F, Wang X, Xu C, Zhang Z, Shi G, Qu L (2014) Graphitic carbon nitride nanoribbons: graphene-assisted formation and synergic function for highly efficient hydrogen evolution. *Angew Chem Int Ed* 50:13934–13939
- [57] Chen L, Huang D, Ren S, Dong T, Chi Y, Chen G (2013) Preparation of graphite-like carbon nitride nanoflake film with strong fluorescent and electrochemiluminescent activity. *Nanoscale* 5:225–230
- [58] Ye L, Wang D, Chen S (2016) Fabrication and enhanced photoelectrochemical performance of MoS₂/S-doped g-C₃N₄ heterojunction film. *ACS Appl Mater Interfaces* 8(8):5280–5289
- [59] Chang Y, Hong F, He C, Zhang Q, Liu J (2013) Nitrogen and sulfur dual-doped non-noble catalyst using fluidic acrylonitrile telomer as precursor for efficient oxygen reduction. *Adv Mater* 25(34):4794–4799
- [60] Guo S, Deng Z, Li M, Jiang B, Tian C, Pan Q, Fu H (2016) Phosphorus-doped carbon nitride tubes with a layered micronanostructure for enhanced visible-light photocatalytic hydrogen evolution. *Angew Chem Int Ed* 55(5):1830–1834
- [61] Chen W, Liu T, Huang T, Liu X, Yang X (2016) Novel mesoporous P-doped graphitic carbon nitride nanosheets coupled with ZnIn₂S₄ nanosheets as efficient visible light driven heterostructures with remarkably enhanced photo-reduction activity. *Nanoscale* 8(6):3711–3719

- [62] Saha S, Sarkar P (2016) Differential pulse anodic stripping voltammetry for detection of As (III) by Chitosan-Fe(OH)₃ modified glassy carbon electrode: a new approach towards speciation of arsenic. *Talanta* 158:235–245
- [63] Cheng F, Yan J, Zhou C, Chen B, Li P, Chen Z, Dong X (2016) An alkali treating strategy for the colloidalization of graphitic carbon nitride and its excellent photocatalytic performance. *J Colloid Interface Sci* 468:103–109
- [64] Xu B, Wang X, Zhu C, Ran X, Li T, Guo L (2017) Probing the inhomogeneity and intermediates in the photosensitized degradation of rhodamine B by Ag₃PO₄ nanoparticles from an ensemble to a single molecule approach. *RSC Adv* 7:40896–40904
- [65] Zhou C, Luo J, Chen Q, Jiang Y, Dong X, Cui F (2015) Titanate nanosheets as highly efficient non-light-driven catalysts for degradation of organic dyes. *Chem Commun* 51:10847–10849
- [66] Jun Y, Lee E, Wang X, Hong W, Stucky G, Thomas A (2013) From melamine-cyanuric acid supramolecular aggregates to carbon nitride hollow spheres. *Adv Funct Mater* 23:3661–3667
- [67] Takizawa T, Watanabe T, Honda K (1978) Photocatalysis through excitation of adsorbates. 2. A comparative study of rhodamine B and methylene blue on cadmium sulfide. *J Phys Chem* 82:1391–1396